Dalton Transactions

PAPER

View Article Online
View Journal

Cite this: DOI: 10.1039/c8dt03801e

Unveiling reactive metal sites in a Pd pincer MOF: insights into Lewis acid and pore selective catalysis†

Benjamin R. Reiner, Abebu A. Kassie and Casey R. Wade *

Received 19th September 2018,
Accepted 13th November 2018

DOI: 10.1039/c8dt03801e

rsc.li/dalton

A porous Zr metal–organic framework, **1-PdBF$_4$** [$Zr_6O_4(OH)_4(OAc)_{2.4}\{(P^NN^NP)Pd(MeCN)\}_{2.4}(BF_4)_{2.4}$; P^NN^NP = 2,6-$(HNPAr_2)_2C_5H_3N$; Ar = *p*-$C_6H_4CO_2^-$], has been synthesized *via* postsynthetic oxidative I^-/BF_4^- ligand exchange using $NOBF_4$. **1-PdBF$_4$** enjoys markedly superior catalytic activity and recyclability to its trifluoracetate-exchanged analogue, **1-PdTFA**, for the intramolecular cyclization of *o*-alkynyl anilines and the carbonyl–ene cyclization of citronellal. Moreover, **1-PdBF$_4$** demonstrates a rare example of pore selective catalysis for the cyclization of 2-ethynyl aniline.

Introduction

Metal–organic frameworks (MOFs) provide attractive scaffolds for heterogeneous catalysis owing to their crystalline structures, inherent porosity, and impressive modularity.[1–6] The immobilization of well-defined reactive sites modelled after molecular catalysts within MOFs offers some unique benefits and challenges. In addition to ease of product separation and recyclability, catalyst site isolation can suppress deactivation pathways leading to improved activity and lifetime *versus* homogeneous analogues.[7–10] On the other hand, complex design strategies and synthetic methods are often needed to effectively heterogenize molecular systems. Moreover, modes of reactivity may not directly translate from homogeneous analogues owing to confinement effects and diffusion limitations.

Pore size and shape optimization have been used to tune host–guest interactions in MOFs for gas storage and molecular separation applications.[11–15] However, there are relatively few reports in which the shape or size of MOF pores have been used to govern product selectivity in catalysis. This is in contrast to zeolites which have a well-documented precedent for shape selective reactivity.[16–19] In fact, the petrochemical industry often employs zeolites for selective catalytic applications including paraffin cracking, skeletal rearrangements, and hydroarylation reactions.[20] MOFs should be ideal platforms for shape-selective catalysis owing to their tunable structures and porosity which can be used to accommodate product-determining transition states or intermediates. Unfortunately, shape-selective catalysis in MOFs remains underexplored. Wang and coworkers have demonstrated pore selective aldol oligomerizations using MIL-101 containing encapsulated phosphotungstic acid (PTA).[21] The PTA molecules effectively restrict the accessible space within the MOF cages, leading to higher selectivity for mono-condensation products with increasing concentrations of PTA. Additionally, Farha, Notestein, and coworkers have reported that PTA-impregnated NU-1000 is selective for intermolecular xylene disproportionation over intramolecular isomerization owing to the presence of adjacent active sites in the confined pore space of the MOF.[22] Liu and Smit have developed a free energy relationship between the selectivity of propene dimerization and the pore size of nanoporous MOF catalysts.[23] Linear selectivity increases in materials with pore sizes that are commensurate with the size of the linear isomers while the formation of branched products is suppressed owing to steric hindrance.

Our group has an ongoing interest in the synthesis and reactivity of MOFs assembled from transition metal diphosphine pincer complexes (Pincer MOFs).[24,25] Pincer complexes are ubiquitous in homogeneous catalysis owing to their tunability and stability, but can benefit from the effects of immobilization and site isolation. We recently reported the synthesis and characterization of **1-PdX** (Scheme 1).[25] A series of postsynthetic modification steps were used to carry out X^-/TFA^- (TFA^- = $CF_3CO_2^-$) ligand exchange at the pincer Pd sites to generate **1-PdTFA**. The oxidative I^-/TFA^- ligand exchange step proceeded to only ~50% yield, even upon successive treatment with the hypervalent iodine reagent $PhI(TFA)_2$. **1-PdTFA** showed good catalytic activity for intramolecular hydroamination of an *o*-substituted alkynyl aniline, but suffered from poor recyclability. An off-cycle reaction pathway resulting in con-

Department of Chemistry and Biochemistry, 100 West 18th Ave, The Ohio State University, Columbus, OH 43210, USA. E-mail: wade.521@osu.edu

†Electronic supplementary information (ESI) available: Spectroscopic (NMR, IR, XRF), crystallographic (PXRD), gas sorption, and GC-MS characterization. See DOI: 10.1039/c8dt03801e

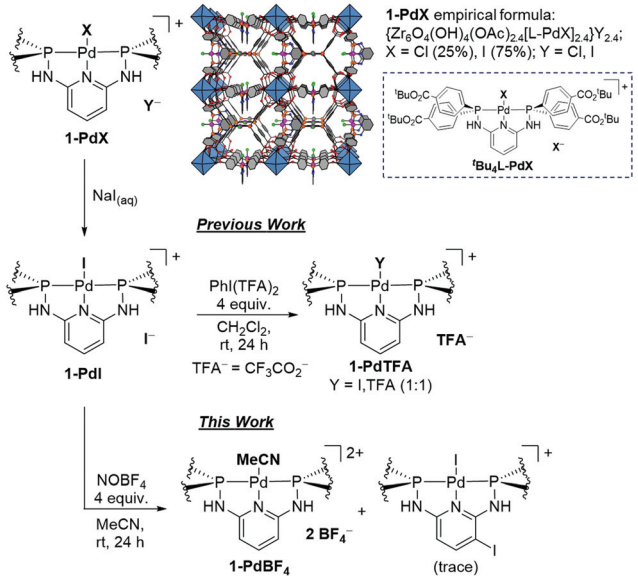

Scheme 1 Synthesis of **1-PdTFA** and **1-PdBF$_4$**.

sumption of the TFA^- counteranions *via* formation of a trifluoroacetamide side product was linked to catalyst deactivation. Comparison of catalytic activity of homogeneous analogues indicated that substitution of TFA^- for a less reactive anion could inhibit catalyst deactivation and improve activity and recyclability. Herein, we report the synthesis of **1-PdBF$_4$** *via* oxidative I^-/BF_4^- ligand exchange using the commercially available reagent $NOBF_4$. This reagent offers a convenient means of activating heterogeneous metal iodide groups for catalysis by introducing a very weakly coordinating BF_4^- counterion. In line with this notion, **1-PdBF$_4$** shows markedly improved Lewis acid catalytic activity and recyclability compared to **1-PdTFA** for intramolecular hydroamination of 2-(butyn-1-yl)aniline and the carbonyl–ene cyclization of citronellal. Moreover, **1-PdBF$_4$** exhibits a high degree of selectivity for the intramolecular hydroamination of 2-ethynylaniline over a self-dimerization process.

Results and discussion

1-PdTFA was previously generated by treating **1-PdX** with NaI followed by $PhI(TFA)_2$ (Scheme 1). The hypervalent iodine reagent effects I^-/TFA^- ligand exchange by oxidation of I^- to I_2, delivering TFA^- as a more weakly coordinating anionic ligand and iodobenzene as a soluble byproduct. The inaccessibility of iodinanes capable of delivering anions that are more weakly coordinating than TFA^- prompted us to consider the use of other oxidants. The homogeneous complexes **^{t}BuL-PdCl** and **^{t}BuL-PdI** were evaluated by cyclic voltammetry (CV) in order to gauge the oxidation potential of the inner and outer sphere I^- ligands (Fig. 1). **^{t}BuL-PdI** features two quasi-reversible oxidations at +0.04 V and +0.34 V *versus* the ferrocene/ferrocenium ($Fc^{0/+}$) couple that are assigned to outer sphere and

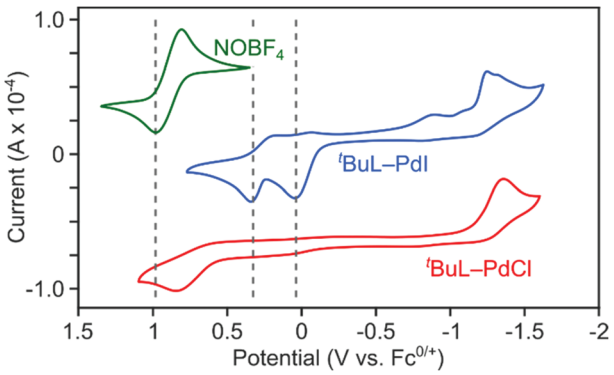

Fig. 1 Cyclic voltammograms of **^{t}BuL-PdCl** (red), **^{t}BuL-PdI** (blue), and $NOBF_4$ (green) in MeCN solution. All measurements were performed using 1 mM analyte and 0.1 M $[^nBu_4N]PF_6$ as supporting electrolyte at a scan rate of 100 mV s^{-1}.

inner sphere iodide oxidation, respectively. Notably, both redox processes occur at more positive potentials than that reported for the free I^-/I_2 couple in the same solvent (~−0.14 V *versus* $Fc^{0/+}$).[26] These current deflections are absent in the voltammogram of **^{t}BuL-PdCl**, which exhibits one irreversible oxidation at +0.83 V. Irreversible reductions are also observed at −0.94 V and −1.24 V for **^{t}BuL-PdI** and at −1.36 V for **^{t}BuL-PdCl**. The ill-defined character of these waves is likely due to halide labilization upon reduction of the complex.

Based on these results, oxidizing agents with redox potentials of ≥+0.40 V *versus* $Fc^{0/+}$ should be sufficient for oxidative abstraction of the I^- ligands in **1-PdI**, with a ~60 mV overpotential necessary to drive the redox equilibrium. Thus, $NOBF_4$ ($E_{1/2}$ = +0.870 V *vs.* $Fc^{0/+}$) was identified as a potentially suitable oxidant for I^-/BF_4^- oxidative ligand exchange of the Pd–I species. Additionally, BF_4^- is one of the smallest weakly coordinating anions with a crystallographic volume of 53 Å^3.[27] For comparison, OTf^- and PF_6^- occupy 85 Å^3 and 75 Å^3 respectively. The use of small counteranions is advantageous since congested pores can preclude efficient ingress and egress of substrates to and from catalytic centers in the MOF.

Synthesis and characterization

1-PdBF$_4$ was synthesized by successive treatment of **1-PdI** with MeCN solutions of $NOBF_4$ at room temperature (Scheme 1). After the first treatment, the supernatant turned a bright orange color. Although nitrosyl iodide (I–NO) is a presumed product of the reaction, it is reported to be unstable at room temperature and should decompose to I_2 and NO.[28,29] Analysis of the isolated solid by X-ray fluorescence (XRF) spectroscopy showed a substantial decrease in the signal arising from the I $K\alpha_1$ emission line (Fig. S1, ESI†). A pale orange supernatant resulted following the second soak, and XRF spectroscopy of the isolated solid showed near complete disappearance of the signal associated with iodine. Elemental analysis data revealed that only trace iodine (<0.25 wt%) remained in the product, corroborating virtually complete I^- substitution. PXRD analysis

confirmed that **1-PdBF$_4$** retains bulk crystallinity after the exchange reaction (Fig. S2, ESI†). Moreover, N_2 adsorption measurements (77 K) provided a calculated Brunauer–Emmett–Teller (BET) surface area of 733 $m^2\ g^{-1}$ for **1-PdBF$_4$**, which is slightly lower than the surface area found for **1-PdI** (922 $m^2\ g^{-1}$) and consistent with substitution of I^- for the larger BF_4^- (Fig. S4, ESI†). Pore size distribution analyses for **1-PdBF$_4$** using the nonlocal density functional theory (NLDFT) method show major pore distributions around 10–12 Å (Fig. S5, ESI†).[30–32]

A sample of **1-PdBF$_4$** was digested with a 3 : 1 v : v mixture of trifluoroacetic acid (HTFA) and C_6D_6, and the resulting solution was analysed by ^{1}H and ^{31}P NMR spectroscopy. The ^{31}P{^{1}H} NMR spectrum features two singlets centered at 76.2 and 70.2 ppm that appear in a ~3.5 : 1 ratio as well as two minor resonances (<5%) at 75.2 and 74.5 ppm (Fig. 2). Addition of a small amount of water to the NMR sample results in disappearance of the downfield signal at 76.2 ppm with a concomitant increase in the intensity of the signal at 70.2 ppm (Fig. S8, ESI†). The minor resonances at 75.2 and 74.5 ppm remain unaffected. Accordingly, the species at 76.2 ppm is assigned to H_4[L-Pd(MeCN)]$^{2+}$, while the signal at 70.2 ppm is attributed to H_4[L-PdOH]$^+$ resulting from reaction of H_4[L-Pd(MeCN)]$^+$ with H_2O present in digestion conditions. The minor resonances are attributed to pincer species resulting from partial iodination of the pyridyl backbone (Scheme 1). The corresponding ^{1}H NMR spectra are consistent with these assignments (Fig. S6 ESI†). The ^{31}P{^{1}H} NMR spectrum of the analogous homogeneous complex, **^{t}Bu$_4$L-PdBF$_4$**, also displays two peaks in the HTFA : C_6D_6 solvent mixture at 76.0 and 71.3 ppm (Fig. S9, ESI†). However, the same complex features only one ^{31}P NMR resonance at 75.9 ppm when the spectrum is collected in anhydrous CH_2Cl_2 (Fig. S10, ESI†), supporting the proclivity of the (P^NN^NP)Pd–MeCN species to hydrolyze under the digestion conditions. The IR spectrum of **1-PdBF$_4$** does not feature any signals attributable to formation of a metal nitrosyl species, but a band at 1222 cm^{-1} that is not present in the spectrum of **1-PdI** can be assigned as the B–F stretch of BF_4^- (Fig. S3, ESI†). Although a ν(CN) band corresponding to Pd-coordinated MeCN is not observed in the ATR-IR spectrum of **1-PdBF$_4$**, ^{1}H NMR spectra of activated samples show the presence of MeCN in a ~1 : 1 ratio with the pincer complexes, supporting its role as an ancillary ligand (Fig. S31 ESI†). Overall, the characterization data points to near full conversion of the Pd–I sites to Pd–MeCN species without any substantial loss in structural integrity.

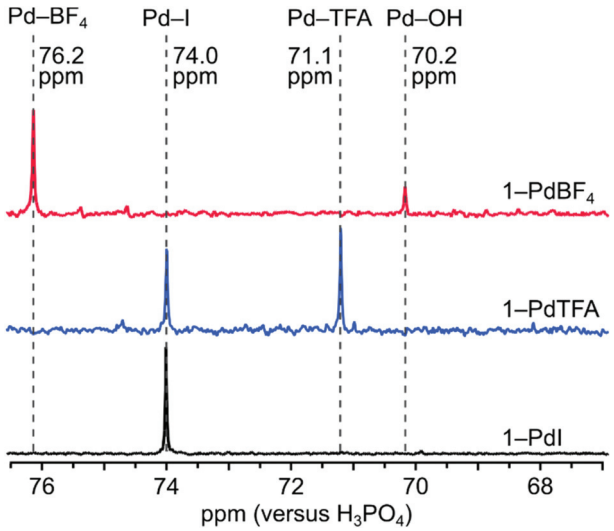

Fig. 2 ^{31}P{^{1}H} NMR spectra of acid-digested (3:1 HTFA:C_6D_6) samples of **1-PdBF$_4$**, **1-PdTFA**, and **1-PdI**.

Catalytic studies

Based on our previous studies with **1-PdTFA**, the intramolecular cyclization of 2-(butyn-1-yl)aniline (**2**) was chosen as a benchmark reaction to evaluate the Lewis acid catalytic activity of **1-PdBF$_4$**.[25] Catalytic reactions were carried out in 1,4-dioxane at 95 °C with 5 mol% catalyst based on Pd (Table 1). Product yields were determined by integration of the ^{1}H NMR spectra with respect to an internal standard (hexamethylbenzene). Under the catalytic conditions, **1-PdI** and **1-PdX** delivered 2-ethylindole **3** in 27% and 41% yield, respectively, after 4 hours (entries 5 and 6), which is consistent with previously observed trends.[25] **1-PdTFA** afforded **3** in only 54% yield (entry 4). **1-PdBF$_4$** proved to be the best catalyst in the series, furnishing **3** in 99% yield (entry 1).

A hot filtration test was performed by separating **1-PdBF$_4$** from the reaction mixture after 30 min and 43% substrate conversion. The filtrate showed only a slight increase in substrate conversion (46%) after continued heating at 95 °C for 3.5 h, supporting the heterogeneous nature of the catalysis (Fig. S32, ESI†). ICP-MS analysis revealed ~0.15 mol% (with respect to substrate) of soluble Pd present in the filtrate solution, which corresponds to leaching of ~3% of the total Pd introduced with the MOF catalyst. Despite a small amount of Pd leaching

Table 1 Hydroamination of *o*-alkynyl aniline **2**[a]

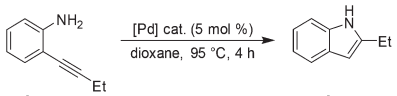

2 **3**

Entry	Catalyst	% Yield **3**[b]	TON[c]	Temp. (°C)
1	**1-PdBF$_4$**	99	20	95
2	**1-PdBF$_4$** (run 5)	92	18	95
3	**1-PdBF$_4$**[d]	84	168	95
4	**1-PdTFA**	54	11	95
5	**1-PdX**	41	8	95
6	**1-PdI**	27	5	95
7	^{t}Bu$_4$L-PdBF$_4$	99	20	25
8	**1-PdBF$_4$**	0	0	25

[a] Reaction conditions: Substrate (0.1 mmol), catalyst (0.005 mmol Pd), 1,4-dioxane, 95 °C, 4 h. [b] Determined by ^{1}H NMR with respect to an internal standard (hexamethylbenzene). [c] Turnover numbers (TON) were calculated per Pd using the empirical formula for **1-PdX** that accounts for missing linker defects. [d] Reaction conducted with 0.5 mol% Pd for 12 hours.

in the initial catalytic run, **1-PdBF$_4$** could be recycled up to five times without any substantial decrease in activity (entry 2). Moreover, PXRD analysis of the MOF following catalysis showed no loss of crystallinity (Fig. S2, ESI†). These results together with the hot filtration test corroborate the stability of **1-PdBF$_4$** toward the catalytic reaction conditions and strongly dispute the role of soluble Pd species as the actuating catalyst. Notably, the MOF catalyst remained competent with loadings as low as 0.5 mol%, delivering **3** in 84% yield (entry 3). We attribute the considerable increase in catalytic activity of **1-PdBF$_4$** over **1-PdTFA** to two factors: an increase in the density of catalytic sites owing to near complete I^-/BF_4^- exchange and suppression of the catalyst deactivation pathway that was previously ascribed to the presence of TFA^-. The catalytic activity of the homogeneous complex **^{t}Bu$_4$L-PdBF$_4$** was also investigated. The complex was synthesized *via* oxidative halide exchange with $NOBF_4$ to eschew any complications associated with adventitious Ag^+ based co-catalysis. **^{t}Bu$_4$L-PdBF$_4$** was markedly superior to **1-PdBF$_4$**, generating indole **3** in 99% yield after 4 h at *room temperature* (entry 7). **1-PdBF$_4$**, however, exhibited no catalytic activity under identical conditions (entry 8).

The interconnected pores (~10 × 16 Å) of **1-PdBF$_4$** are sufficiently large to accommodate **2** and **3**, which have kinetic diameters of ~9–10 Å. However, the large discrepancy in catalytic activity between **1-PdBF$_4$** and **^{t}Bu$_4$L-PdBF$_4$** suggests that there may be substrate/product diffusion limitations in the MOF. In order to gain further insight, the cyclization of **2** was monitored as a function of time for each catalyst using GC-FID to quantify substrate conversion. The reaction catalysed by **1-PdBF$_4$** initially proceeds at a relatively fast rate, but decelerates to a regime that appears zero order in substrate (Fig. 3a). The full reaction profile could not be satisfactorily fit using a single term exponential function (Fig. S18, ESI†). While this unusual behaviour was reproducible over multiple samples of freshly prepared **1-PdBF$_4$**, recycling the catalyst revealed a dramatic change to a linear reaction profile, which is consistent with mass transport limitations. The slope extracted from linear least-squares fitting of the second run matches the slope of the slow kinetic regime (t = 20–120 min) observed during the first run (Fig. 3a). Thus, the change in reaction profile for pristine **1-PdBF$_4$** after ~30 min implies that the species responsible for the fast initial rate are quickly deactivated. The leached Pd observed in the filtrate after the hot filtration is a likely culprit, but we cannot rule out the possibility that missing linker defect sites in the MOF or other immobilized species are responsible for the aberrant kinetic behaviour. Although the identity of the fleeting catalyst species has not been fully elucidated, its influence on the initial reaction rate underscores the importance of measuring reaction kinetics on pristine and recycled samples in order to accurately evaluate the catalytic behaviour of novel materials.[33]

The reaction catalysed by **^{t}Bu$_4$L-PdBF$_4$** displays the exponential decay expected for first order kinetics (Fig. 3b), but a plot of ln[2] *vs.* time shows clear deviation from linearity. This behaviour is attributed to decomposition of the catalyst over time, which is supported by the appearance of multiple phosphorus-containing species by ^{31}P NMR spectroscopy as well as the formation of metal mirrors on reaction vessels following catalytic reactions. Diffusion-limited behaviour is not evident in the observed kinetic profile for reactions catalysed by **^{t}Bu$_4$L-PdBF$_4$**. The fact that the reaction catalysed by **1-PdBF$_4$** appears zero order in substrate is indicative of mass transport limitations and is consistent with the catalysis occurring, at least in part, within the pores of the MOF. Unfortunately, **1-PdBF$_4$** has only been obtained as a fine microcrystalline powder, making it difficult to measure reaction rate as a function of crystallite size.

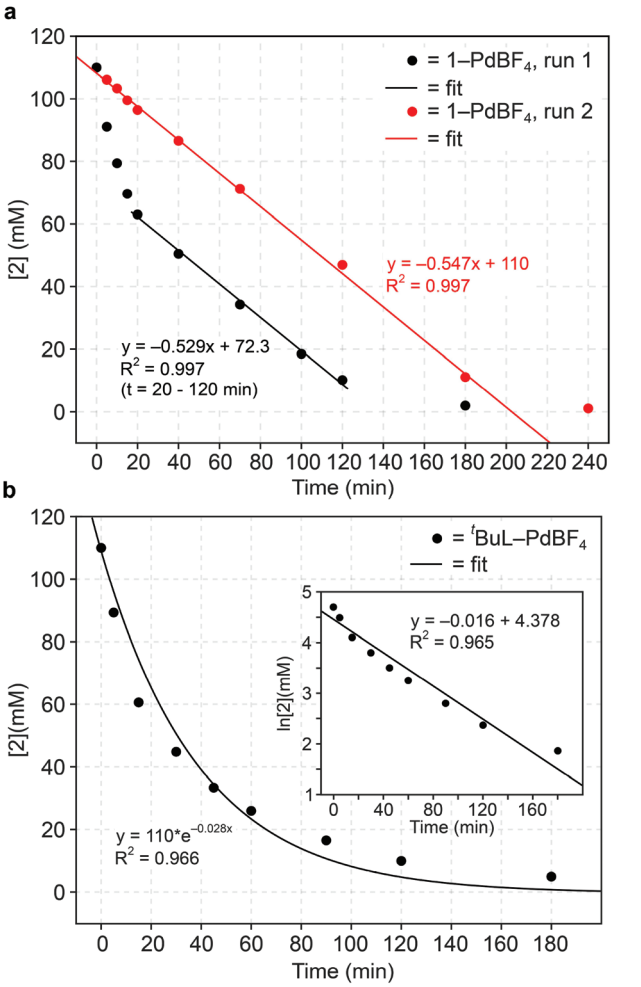

Fig. 3 Reaction profile for cyclization of **2** in the presence of (a) **1-PdBF$_4$** at 95 °C or (b) **^{t}Bu$_4$L-PdBF$_4$** at 25 °C. The inset in (b) is a plot of ln [**2**] *vs.* time that shows the deviation from linearity and first order kinetic behaviour.

We considered that the confined environment around the Pd pincer sites of **1-PdBF$_4$** might be leveraged toward pore selective transformations. More specifically, **1-PdBF$_4$** should be expected to favor intramolecular over intermolecular reactions while the homogenous analogue, **^{t}BuL-PdBF$_4$**, would lack similar control over the reaction selectivity. 2-Ethynyl aniline **4** was chosen as a model substrate to investigate this notion.

4 can undergo an intramolecular hydroamination to form indole **5** or a tandem intermolecular hydroamination–annulation sequence to afford quinoline **6**.[34–36] NLDFT pore size analysis of N_2 adsorption isotherms indicates that **1-PdBF$_4$** contains pores that are ~ 10–12 Å in diameter (Fig. S5, ESI†). Thus, while **4** should be easily accommodated within **1-PdBF$_4$** owing to a relatively small kinetic diameter (~7 Å), the arrangement of two substrate molecules within the pores of **1-PdBF$_4$** to afford quinoline **6** seemed unlikely. Catalytic reactions were carried out in 1,4-dioxane at 95 °C with 5 mol% catalyst based on Pd (Table 2). Product yields were determined by GC-FID.

Initial attempts to catalyze the cyclization of **4** with **^{t}BuL-PdTFA** or **1-PdTFA** were unsuccessful and only stoichiometric amounts of trifluoroacetamide **7** (~10%) were observed. The absence of cyclized products **5** and **6** suggests that the consumption of TFA^- *via* the formation of **7** leads to deactivation of the pincer complexes for catalysis (Table 2, entries 2 and 4). On the other hand, **^{t}BuL-PdBF$_4$** promoted quantitative conversion of **4** after 24 hours, delivering a ~1 : 1 mixture of indole **5** and quinoline **6**. Monitoring the reaction over time showed the selectivity did not change substantially as a function of conversion. The conversion of ethynyl aniline **4** was substantially slower than butynyl aniline **2**, an effect that we attribute to increased substrate inhibition associated with the less sterically congested aniline. Nonetheless, after 60 h, **1-PdBF$_4$** furnished **5** in 65% yield (entry 1) with no detectable amount of **6**. A small amount of aminoacetophenone (<5%) was detected as a consequence of substrate hydration by adventitious water. The observation of **5** as the sole major product demonstrates a rare example of pore selective reactivity in which the microenvironment of the MOF engenders unique selectivity that is not easily attained with an analogous homogenous catalyst.

The carbonyl–ene cyclization of citronellal, **8**, is frequently used as a benchmark for measuring the Lewis acidity of heterogeneous catalyst platforms.[37–41] The diastereoselective cyclization of citronellal to isopulegol is also a key reaction in the synthesis of menthol, a naturally occurring extract of mint leaves with valuable fragrance and pharmaceutical properties. Moreover, recyclable heterogeneous catalysts are attractive substitutes for $ZnBr_2$, which acts as a stoichiometric promoter in the industrial process, but is considered a severe marine toxin. Consequently, the good activity and recyclability of **1-PdBF$_4$** for intramolecular hydroamination prompted us to investigate its efficacy as a catalyst for the cyclization of citronellal. Catalytic reactions were carried out in toluene at 100 °C with 10 mol% catalyst based on Pd (Table 3). Product yields were determined by GC-FID.

After 30 minutes under the catalytic conditions, **1-PdBF$_4$** delivered isopulegol in 64% yield (entry 1) and could be recycled 3 times without any loss in activity (entry 2). Only pulegol isomers were observed and the 67% selectivity toward the isopulegol diastereomer did not improve when the reaction was conducted at lower temperatures. Other MOF catalysts including Cu_3BTC_2 [37,40] and UiO-66[38] have shown comparable selectivity. The parent MOF, **1-PdX**, shows limited activity for this reaction, affording **9** in only 16% yield (entry 3). This result supports the immobilized Pd^{2+} sites as the actuating catalyst since X^-/BF_4^- exchange greatly improves catalytic activity. Moreover, framework defects leading to accessible coordination sites at the Zr nodes do not appear to contribute greatly to the observed catalysis.[38]

The catalytic activity of **1-PdBF$_4$** toward citronellal cyclization was further examined by kinetic analysis. The reaction proceeds too quickly at 10 mol% Pd loading to be easily monitored, so kinetic measurements were carried out at 0.5 mol% Pd loading (Fig. S29, ESI†). At 100 mM substrate concentration, the full reaction profile could be satisfactorily fit with a single term exponential function, indicative of first order kinetics. At 200 mM substrate concentration, initial catalytic runs showed unusually rapid substrate conversion at early reaction times followed by a deceleration (Fig. S30, ESI†). However, the reaction profile for the recycled catalyst fits well to a first order exponential decay, again indicating that catalyti-

Table 2 Cyclization of *o*-ethynyl aniline **4**[a]

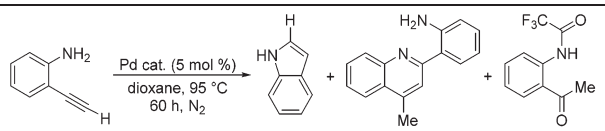

4 5 6 7

Entry	Catalyst	% conversion	% yield **5**[b]	Selectivity (**5** : **6** : **7**)
1	**1-PdBF$_4$**	70	65	65 : 0 : 0
2	**1-PdTFA**	10	0	0 : 0 : 10
3	^{t}Bu$_4$L-PdBF$_4$[c]	100	45[c]	45 : 55 : 0
4	^{t}Bu$_4$L-PdTFA	10	0	0 : 0 : 10

[a] Reaction conditions: Substrate (0.1 mmol), catalyst (0.005 mmol Pd), 1,4-dioxane, 95 °C, 60 h. [b] Determined by GC-FID with respect to an internal standard (hexamethylbenzene). [c] Reaction time was 24 h.

Table 3 Cyclization of citronellal (**8**) to isopulegol (**9**)[a]

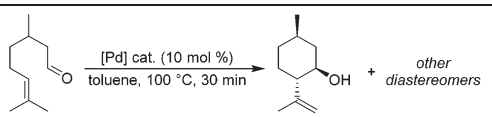

8 9

Entry	Catalyst	% conversion **8**	% yield **9**[b]	TON[d]
1	**1-PdBF$_4$**	100	64	10
2	**1-PdBF$_4$** (run 3)	100	63	10
3	**1-PdX**	17	16	2
4	**1-PdBF$_4$**[c]	96	60	192
5	^{t}Bu$_4$L-PdBF$_4$	100	73	10
6	^{t}Bu$_4$L-PdBF$_4$[c]	71	51	140
7	None	0	0	0

[a] Reaction conditions: Substrate (0.05 mmol), catalyst (0.005 mmol Pd), toluene, 100 °C, 3 h. [b] Determined by GC-FID with respect to an internal standard (hexamethylbenzene). [c] Reaction conducted with 0.5 mol% Pd for 3 hours. [d] Turnover numbers (TON) were calculated per Pd using the empirical formula for **1-PdX** that accounts for missing linker defects. TON refers to total amount of pulegol isomers formed.

cally active, adventitious species are present in freshly prepared samples of **1-PdBF$_4$**. Interestingly, the citronellal isomerization shows first order kinetic behaviour while cyclization of **2** exhibits apparent zero-order behaviour. We surmise that the disparity in kinetic behaviours arises from differences in product release from the framework. Protodemetalation is often the rate-limiting step in homogeneously catalysed, intramolecular hydroamination reactions.[42,43] This step may be substantially hindered by the confined environment of the MOF, leading to slow release of indole **3** from the framework and the apparent zero order behaviour. Citronellal cyclization reactions carried out with an initial substrate concentration of 200 mM show an average TOF of 144 h^{-1} after 1 h reaction time, which is among the highest reaction rates reported using MOF-based catalysts.[37–41,44]

The cyclization of citronellal was also examined using the homogeneous analogue **^{t}Bu$_4$L-PdBF$_4$** (0.5 mol%) as a catalyst. After 3 h, only 71% of the starting material had been converted, delivering the desired isopulegol diastereomer **9** in 51% yield (entry 5). In comparison, **1-PdBF$_4$** furnishes **9** in 60% yield concomitant with nearly quantitative citronellal conversion in the same time period (entry 4). During the course of the reaction, **^{t}Bu$_4$L-PdBF$_4$** appears to decompose *via* reduction to Pd(0) as evidenced by the formation of metal mirrors on reaction vessels following catalytic reactions. Thus while **1-PdBF$_4$** showed lower catalytic activity than **^{t}Bu$_4$L-PdBF$_4$** for the intramolecular hydroamination of **2**, it performs slightly better than the homogeneous analogue for the cyclization of **8**. Morever, **1-PdBF$_4$** can be recycled at least 3 times without loss of activity, suggesting that immobilization of the Pd P^{N}N^{N}P complexes within **1-PdBF$_4$** suppress deleterious reductive processes that decrease catalyst lifetime.

Conclusions

NOBF$_4$ has been employed as a reagent for I$^-$/BF$_4^-$ oxidative ligand exchange to generate **1-PdBF$_4$** which exhibits significantly better Lewis acid catalytic activity and recyclability than the previously reported TFA$^-$ analogue **1-PdTFA**. The differences in reactivity can be attributed to the more weakly coordinating nature of BF$_4^-$ and its lower propensity to undergo deleterious side reactions with substrates. Moreover, NOBF$_4$ is a stronger oxidant than the hypervalent iodine reagent previously used, leading to more effective oxidation of inner sphere Pd–I species and near quantitative I$^-$/BF$_4^-$ exchange. **1-PdBF$_4$** proved to be a highly recyclable catalyst for the intramolecular hydroamination of 2-(butyn-1-yl)aniline and the carbonyl–ene cyclization of citronellal. While mass transport limitations appear to be present for the intramolecular hydroamination of **2**, the steric constraints of the MOF could be exploited to provide a rare example of pore selective catalysis. With 2-ethynylaniline as a substrate, **1-PdBF$_4$** exclusively delivered the intramolecular hydroamination product **5** while the homogeneous analogue **^{t}Bu$_4$L-PdBF$_4$** generated a mixture of **5** and the intermolecular hydroamination–annulation product **6**. Ongoing work is focused on understanding how product selectivity exhibited by **1-PdBF$_4$** can be extended to other more challenging chemical reactions and elucidating factors that affect the kinetic behavior of **1-PdBF$_4$** and other related MOF catalysts.

Experimental section

General considerations

All manipulations were carried out using a nitrogen-filled glovebox or standard Schlenk techniques unless otherwise noted. All glassware was oven dried in a 150 °C oven before use. Solvents were degassed by sparging with ultra-high purity argon and dried *via* passage through columns of drying agents using a solvent purification system from Pure Process Technologies. 2-Butynyl aniline **2**,[45] 2-ethynyl aniline **4**,[46] PhITFA$_2$,[47] and **1-PdI**[25] were prepared as described in the literature. All other solvents and reagents were purchased from commercial suppliers and used as received.

Powder X-ray diffraction patterns were collected using a Rigaku Miniflex 600 diffractometer with Nickel-filtered Cu-K$_\alpha$ radiation (λ = 1.5418 Å). XRF spectra were collected on an Innov-X Systems X-500 spectrometer using unfiltered Co-K$_\alpha$ radiation (λ = 1.7892 Å). Solution-state NMR spectra were measured using a Bruker DPX 400 MHz spectrometer (162 MHz operating frequency for ^{31}P). For ^{1}H NMR spectra, the residual solvent resonance was referenced as an internal standard. For ^{31}P{^{1}H} NMR spectra, 85% H$_3$PO$_4$ was used as an external standard (0 ppm). Solvent-suppressed ^{1}H NMR spectra were collected using 180° water selective excitation sculpting with default parameters and pulse shapes.[48] Briefly, spectra were collected using selective pulses of 1 ms with the transmitter frequency set to the center of the solvent resonance. The recycle delay between scans was 20 s, 16 K points were collected, and the acquisition time was 2.5 s. Nitrogen adsorption isotherms were measured at 77 K (liquid nitrogen bath) using a Micromeritics 3Flex Surface Characterization Analyzer. Prior to analysis, samples (~100 mg) were heated under reduced pressure until the outgas rate was less than 2 mTorr per minute. GC-MS analysis was performed using an Agilent 7890B GC system equipped with the HP-5 Ultra Inert column (30 m, 0.25 mm, 0.25 μm), and a FID detector. For MS detection an electron ionization system was used with an ionization energy of 70 eV. Elemental microanalyses were performed by Atlantic Microlab (Norcross, GA).

Electrochemistry

Cyclic voltammetry measurements were carried out in a nitrogen-filled glovebox in a one compartment cell using a CH Instruments 600C electrochemical analyzer. A glassy carbon electrode and platinum wire were used as the working and auxiliary electrodes, respectively. A silver wire was used as a pseudoreference electrode, and potentials are reported relative to an internal ferrocene reference. Solutions of electrolyte (0.1 M TBAPF$_6$) and analyte (1 mM) were also prepared in the glovebox.

Synthesis of 1-PdBF$_4$

In a N_2-filled glovebox, a solution of $NOBF_4$ (0.009 g, 0.072 mmol) in MeCN (1 mL) was added to a suspension of **1-PdI** (0.100 g) in MeCN (5 mL) in a 20 mL scintillation vial. The vial was sealed and left gently stirring at room temperature for 12 h. The reaction mixture was centrifuged, and the orange supernatant was decanted. A fresh solution of $NOBF_4$ (0.009 g, 0.072 mmol) in MeCN (6 mL) was added and the reaction again stirred at room temperature for 12 h. The solid was collected by centrifugation, washed with MeCN (3 × 5 mL), and dried briefly *in vacuo*. **1-PdBF$_4$** was isolated as an off-white microcrystalline powder (0.100 g). $^{31}P\{^1H\}$ NMR (162.0 MHz, 3/1 v/v CF_3COOH/C_6D_6): δ 76.2 (s); 75.2 (s); 74.5 (s); 70.2 (s). Anal. calcd for chemical formula: $[Zr_6O_4(OH)_4(OAc)_{2.4}\{(P^NN^NP)Pd(MeCN)\}_{2.4}(BF_4)_{2.4}$ $(C_{88.8}H_{68.8}N_{9.6}O_{12.8}B_{2.4}F_{9.6}Zr_6Pd_{2.4})]$: C, 34.21; H, 2.30; N, 4.31. Found: C, 31.81; H, 2.00; N, 4.10; I, <0.25.

General procedure for catalytic hydroamination reactions with 2 and 4

In a N_2-filled glovebox, a vial was charged with **2** or **4** (0.1 mmol), 5 mol% catalyst, 1,4-dioxane (0.5 mL), C_6D_6 (0.1 mL), and a known amount of hexamethylbenzene (0.005–0.01 mmol) as an internal standard. The reaction mixture was transferred to an NMR tube and heated at 95 °C for 4 h. The product yields were determined by ^1H NMR spectroscopy for **2** (Fig. S11–S17, ESI†) and ^1H NMR spectroscopy or GC-FID for **4** (Fig. S19–S22, ESI†). For recycling experiments, **1-PdBF$_4$** was isolated from the reaction mixture *via* centrifugation, washed with 1,4-dioxane (3 × 2 mL), and resubjected to the reaction conditions described above.

General procedure for carbonyl–ene reactions

In a N_2-filled glovebox, a 1 dram screw-top vial fitted with a Teflon lined cap was charged with **8** (0.05 mmol), 10 mol% catalyst, toluene (2 mL), and a known amount of hexamethyl benzene (0.01–0.04 mmol) as an internal standard. The reaction mixture was heated at 100 °C for 30 minutes. The product yields were determined by GC-FID. For recycling experiments, **1-PdBF$_4$** was isolated from the reaction mixture *via* centrifugation, washed with toluene (3 × 2 mL), and resubjected to the reaction conditions described above.

Conflicts of interest

There are no conflicts to declare.

Acknowledgements

Acknowledgment is made to the Donors of the American Chemical Society Petroleum Research Fund (Grant 55281-DNI-3) for support of this research.

Notes and references

1 J. Lee, O. K. Farha, J. Roberts, K. A. Scheidt, S. T. Nguyen and J. T. Hupp, *Chem. Soc. Rev.*, 2009, **38**, 1450–1459.
2 C. Wang, D. Liu and W. Lin, *J. Am. Chem. Soc.*, 2013, **135**, 13222–13234.
3 A. H. Chughtai, N. Ahmad, H. A. Younus, A. Laypkov and F. Verpoort, *Chem. Soc. Rev.*, 2015, **44**, 6804–6849.
4 S. M. Cohen, Z. Zhang and J. A. Boissonnault, *Inorg. Chem.*, 2016, **55**, 7281–7290.
5 S. M. J. Rogge, A. Bavykina, J. Hajek, H. Garcia, A. I. Olivos-Suarez, A. Sepúlveda-Escribano, A. Vimont, G. Clet, P. Bazin, F. Kapteijn, M. Daturi, E. V. Ramos-Fernandez, F. X. Llabrés i Xamena, V. Van Speybroeck and J. Gascon, *Chem. Soc. Rev.*, 2017, **46**, 3134–3184.
6 Z. Hu and D. Zhao, *CrystEngComm*, 2017, **19**, 4066–4081.
7 S. Pullen, H. Fei, A. Orthaber, S. M. Cohen and S. Ott, *J. Am. Chem. Soc.*, 2013, **135**, 16997–17003.
8 Z. Li, T. M. Rayder, L. Luo, J. A. Byers and C.-K. Tsung, *J. Am. Chem. Soc.*, 2018, **140**, 8082–8085.
9 S. Lin, A. K. Ravari, J. Zhu, P. M. Usov, M. Cai, S. R. Ahrenholtz, Y. Pushkar and A. J. Morris, *ChemSusChem*, 2018, **11**, 464–471.
10 T. Drake, P. Ji and W. Lin, *Acc. Chem. Res.*, 2018, **51**, 2129–2138.
11 J.-R. Li, R. J. Kuppler and H.-C. Zhou, *Chem. Soc. Rev.*, 2009, **38**, 1477–1504.
12 K. Adil, Y. Belmabkhout, R. S. Pillai, A. Cadiau, P. M. Bhatt, A. H. Assen, G. Maurin and M. Eddaoudi, *Chem. Soc. Rev.*, 2017, **46**, 3402–3430.
13 S. Qiu, M. Xue and G. Zhu, *Chem. Soc. Rev.*, 2014, **43**, 6116–6140.
14 H. Furukawa, F. Gándara, Y.-B. Zhang, J. Jiang, W. L. Queen, M. R. Hudson and O. M. Yaghi, *J. Am. Chem. Soc.*, 2014, **136**, 4369–4381.
15 H. Li, K. Wang, Y. Sun, C. T. Lollar, J. Li and H.-C. Zhou, *Mater. Today*, 2018, **21**, 108–121.
16 S. M. Csicsery, *Zeolites*, 1984, **4**, 202–213.
17 J. Jae, G. A. Tompsett, A. J. Foster, K. D. Hammond, S. M. Auerbach, R. F. Lobo and G. W. Huber, *J. Catal.*, 2011, **279**, 257–268.
18 C. Song, J. M. Garcés and Y. Sugi, *ACS Symp. Ser.*, 1999, **738**, 1–16.
19 J. M. Garcés, M. M. Olken, G. John Lee, G. R. Meima, P. A. Jacobs and J. A. Martens, *Top. Catal.*, 2009, **52**, 1175–1181.
20 T. F. Degnan, *J. Catal.*, 2003, **216**, 32–46.
21 Q. Deng, G. Nie, L. Pan, J.-J. J. Zou, X. Zhang and L. Wang, *Green Chem.*, 2015, **17**, 4473–4481.
22 S. Ahn, S. L. Nauert, C. T. Buru, M. Rimoldi, H. Choi, N. M. Schweitzer, J. T. Hupp, O. K. Farha and J. M. Notestein, *J. Am. Chem. Soc.*, 2018, **140**, 8535–8543.
23 Y. M. Liu and B. Smit, *ACS Catal.*, 2017, **7**, 3940–3948.
24 S. A. Burgess, A. Kassie, S. A. Baranowski, K. J. Fritzsching, K. Schmidt-Rohr, C. M. Brown and C. R. Wade, *J. Am. Chem. Soc.*, 2016, **138**, 1780–1783.

25 B. R. Reiner, N. T. Mucha, A. Rothstein, J. S. Temme, P. Duan, K. Schmidt-Rohr, B. M. Foxman and C. R. Wade, *Inorg. Chem.*, 2018, **57**, 2663–2672.
26 N. G. Connelly and W. E. Geiger, *Chem. Rev.*, 1996, **96**, 877–910.
27 J. K. Clegg, J. Cremers, A. J. Hogben, B. Breiner, M. M. J. Smulders, J. D. Thoburn and J. R. Nitschke, *Chem. Sci.*, 2013, **4**, 68–76.
28 L. Dózsa, I. Szilassy and M. T. Beck, *Inorg. Chim. Acta*, 1976, **17**, 147–153.
29 R. Weiß and K.-G. Wagner, *Chem. Ber.*, 1984, **117**, 1973–1976.
30 C. Lastoskie, K. E. Gubbins and N. Quirke, *Langmuir*, 1993, **9**, 2693–2702.
31 C. Lastoskie, K. E. Gubbins and N. Quirke, *J. Phys. Chem.*, 1993, **97**, 4786–4796.
32 P. I. Ravikovitch, G. L. Haller and A. V. Neimark, *Adv. Colloid Interface Sci.*, 1998, **76–77**, 203–226.
33 S. L. Scott, *ACS Catal.*, 2018, 8597–8599.
34 N. Sakai, K. Annaka and T. Konakahara, *J. Org. Chem.*, 2006, **71**, 3653–3655.
35 N. Sakai, K. Annaka, A. Fujita, A. Sato and T. Konakahara, *J. Org. Chem.*, 2008, **73**, 4160–4165.
36 C. Praveen and P. Perumal, *Synthesis*, 2016, **48**, 855–864.
37 L. Alaerts, E. Séguin, H. Poelman, F. Thibault-Starzyk, P. A. Jacobs and D. E. De Vos, *Chem. – Eur. J.*, 2006, **12**, 7353–7363.
38 F. Vermoortele, M. Vandichel, B. Van De Voorde, R. Ameloot, M. Waroquier, V. Van Speybroeck and D. E. De Vos, *Angew. Chem., Int. Ed.*, 2012, **51**, 4887–4890.
39 F. G. Cirujano, *Catal. Sci. Technol.*, 2017, **7**, 5482–5494.
40 M. Vandichel, F. Vermoortele, S. Cottenie, D. E. De Vos, M. Waroquier and V. Van Speybroeck, *J. Catal.*, 2013, **305**, 118–129.
41 F. G. Cirujano, F. X. Llabrés I Xamena and A. Corma, *Dalton Trans.*, 2012, **41**, 4249–4254.
42 B. M. Cochran and F. E. Michael, *J. Am. Chem. Soc.*, 2008, **130**, 2786–2792.
43 L. Huang, M. Arndt, K. Gooßen, H. Heydt and L. J. Gooßen, *Chem. Rev.*, 2015, **115**, 2596–2697.
44 J. Jiang, F. Gándara, Y.-B. Zhang, K. Na, O. M. Yaghi and W. G. Klemperer, *J. Am. Chem. Soc.*, 2014, **136**, 12844–12847.
45 C. Maaliki, Y. Chevalier, E. Thiery and J. Thibonnet, *Tetrahedron Lett.*, 2016, **57**, 3358–3362.
46 N. Sakai, K. Tamura, K. Shimamura, R. Ikeda and T. Konakahara, *Org. Lett.*, 2012, **14**, 836–839.
47 A. A. Zagulyaeva, M. S. Yusubov and V. V. Zhdankin, *J. Org. Chem.*, 2010, **75**, 2119–2122.
48 T. L. Hwang and A. J. Shaka, *J. Magn. Reson., Ser. A*, 1995, **112**, 275–279.

